Characterization of the copper(II) binding site in the pink copper binding protein CusF by electron paramagnetic resonance spectroscopy. J Biol Inorg Chem

ARTICLE *in* JBIC JOURNAL OF BIOLOGICAL INORGANIC CHEMISTRY · JUNE 2005

Impact Factor: 2.54 · DOI: 10.1007/s00775-005-0631-y · Source: PubMed

5 AUTHORS, INCLUDING:

Arnold M Raitsimring
The University of Arizona
123 PUBLICATIONS **2,574** CITATIONS
SEE PROFILE

F(rances) Ann Walker
The University of Arizona
240 PUBLICATIONS **8,640** CITATIONS
SEE PROFILE

Christopher Rensing
University of Copenhagen
140 PUBLICATIONS **5,692** CITATIONS
SEE PROFILE

Megan M Mcevoy
The University of Arizona
36 PUBLICATIONS **1,035** CITATIONS
SEE PROFILE

J Biol Inorg Chem (2005) 10: 221–230
DOI 10.1007/s00775-005-0631-y

ORIGINAL ARTICLE

Andrei V. Astashkin · Arnold M. Raitsimring
F. Ann. Walker · Christopher Rensing
Megan M. McEvoy

Characterization of the copper(II) binding site in the pink copper binding protein CusF by electron paramagnetic resonance spectroscopy

Received: 15 October 2004 / Accepted: 1 February 2005 / Published online: 16 March 2005

Abstract Electron paramagnetic resonance (EPR) spectroscopy has been used to structurally characterize the copper-binding site in CusF protein from *Escherichia coli*. The EPR spectra indicate a single type II copper center with parameters typical for nitrogen and oxygen ligands ($A_{\parallel}$~200 G, $g_{\parallel}$~2.186, $g_{\perp}$~2.051). The pulsed EPR data show that one of the ligands to Cu^{2+} is an imidazole ring of a histidine residue. The remote amino nitrogen of this imidazole ring is readily observed by electron spin-echo envelope modulation spectroscopy, while the imino nitrogen that is directly coordinated to the Cu^{2+} ion is observed by pulsed electron–nuclear double resonance (ENDOR). In addition, the ENDOR spectra reveal the presence of one more nitrogen ligand that was assigned to be a deprotonated peptide nitrogen. Apart from the two nitrogen ligands, it has been established that there are two nearby hydroxyl protons, although whether these belong to a single equatorial water ligand or two equatorial hydroxide ligands is not known.

Keywords Copper homeostasis · Electron paramagnetic resonance spectroscopy

A. V. Astashkin · A. M. Raitsimring · F. A. Walker
Department of Chemistry, University of Arizona, Tucson, AZ 85721, USA

C. Rensing
Department of Soil, Water and Environmental Science, University of Arizona, Tucson, AZ 85721, USA

M. M. McEvoy (✉)
Department of Biochemistry and Molecular Biophysics, University of Arizona, Tucson, AZ 85721, USA
E-mail: mcevoy@email.arizona.edu
Tel.: +1-520-6213489
Fax: +1-520-6211697

Introduction

Copper is an essential element for most living organisms, although an excess of copper can be detrimental. Owing to the ease with which it changes redox states, copper is a component of a number of essential enzymes; however, this same redox reactivity can create free radicals, which are extremely damaging to cells. Accordingly, several mechanisms exist in cells to carefully regulate copper levels. In *Escherichia coli* one of these systems is the *cus* determinant, which confers copper and silver resistance to the cells. Transcription of the genes encoding the CusCFBA proteins is increased in response to both silver and copper [1, 2].

The CusCBA proteins are expected to form a three-component, chemiosmotic, cation/proton antiporter for removal of copper from the cell on the basis of the similarity of their sequences to other systems [3]. Antiporters of this type are found throughout bacteria, and are used to export drugs, metals, and xenobiotics. The sequence of CusA indicates that it is a member of the resistance/nodulation/division (RND) protein superfamily. Proteins in this family couple the movement of protons across the inner bacterial membrane with the export of the substrate. CusB is a member of the family of membrane fusion proteins, which are located primarily in the periplasmic space between the inner and outer membranes of gram-negative bacteria. CusC is an outer membrane factor, which forms a channel from the periplasm to the extracellular space. The *cus* determinant also contains an additional gene, *cusF*, needed for maximal copper resistance [2]. CusF is a novel addition to this system, and has only been reported in other copper/silver transport systems [4]. The exact function of CusF is unknown, but it may serve as a periplasmic metallochaperone to deliver copper from the periplasm to the CusCBA efflux complex.

CusF has an unusual absorbance maximum at approximately 510 nm ($\epsilon = 114\ M^{-1}\ cm^{-1}$), a shoulder on the UV absorbance at approximately 390 nm, and a

pink color when purified [2]. These properties are suggestive of an unusual coordination environment for the copper. Of the types of protein side chains that typically act as ligands to copper, the mature processed sequence of CusF contains five histidines, no cysteines, and four methionines as well as two additional histidines from the C-terminal affinity purification tag [2].

CusF has no close sequence homologs, apart from hypothetical proteins from other presumed copper/silver transport systems, and therefore little can be surmised about its function from studies of related proteins. To elucidate the function of CusF, we have sought to characterize the copper environment using continuous wave (CW) and pulsed electron paramagnetic resonance (EPR) spectroscopy.

Materials and methods

CusF protein was expressed from the pASK-IBA3 plasmid in *E. coli* BL21-DE3 and purified as previously described [2]. Uniformly ^{15}N-labeled CusF was obtained from M9 minimal media containing $^{15}NH_4Cl$ as the sole nitrogen source.

Samples for EPR spectroscopy ranged from 0.8–1 mM CusF in 5 mM tris(hydroxymethyl)aminomethane (Tris)–HCl, pH 8.0, 10 mM NaCl, and 50% glycerol in H_2O. To prepare the CusF sample in D_2O, an aliquot of 1.8 mM CusF in 10 mM Tris–HCl, pH 8.0, 20 mM NaCl was frozen in liquid nitrogen and lyophilized. The lyophilized protein was resuspended in a 1:1 mixture of D_2O and glycerol- d_8, giving a final concentration of 0.9 mM CusF.

CW EPR spectra were measured on a Bruker ESP-300E X-band EPR spectrometer, at 77 K, using an immersion Dewar. Electron spin-echo envelope modulation (ESEEM) and pulsed electron–nuclear double resonance (ENDOR) experiments were performed on a homebuilt pulsed EPR spectrometer operating in the microwave (mw) frequency range from 8 to 18 GHz (X and K_u bands) and equipped with a helium-flow cryostat (Oxford, CF935) and a pulsed ENDOR accessory. The X-band cylindrical dielectric ENDOR resonator was described earlier [5], and the K_u-band resonator was similar in design but had smaller overall dimensions and, consequently, higher resonance frequencies. A RF amplifier (Amplifier Research, AR-250L) provided a nominal output power of about 1 kW in the pulsed mode. The measurement temperature was about 20 K.

Results

EPR field sweep spectra

Trace 1 in Fig. 1shows a K_u band primary electron spin-echo detected field sweep spectrum of CusF. A numerical simulation of this spectrum (trace 2 in Fig. 1) results in the following parameters: $g_{\|}\approx 2.186$, $g_{\perp}\approx 2.051$,

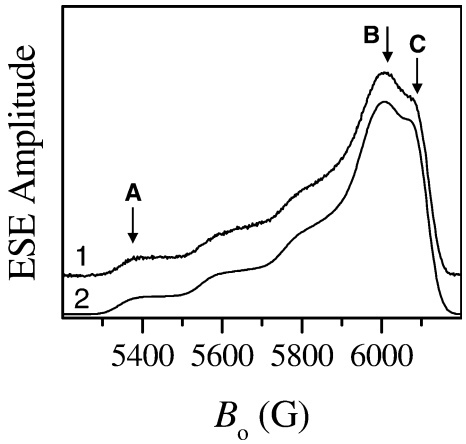

Fig. 1 *Trace 1*, field sweep spectrum of CusF recorded using the primary electron spin-echo (*ESE*) sequence. *Arrows* marked *A*, *B* and *C*indicate the spectrum positions where the ESE envelope modulation (*ESEEM*) and pulsed electron–nuclear double resonance (*ENDOR*) experiments were performed. Experimental conditions: microwave (*mw*) frequency, 17.285 GHz; mw pulses, 2×10 ns; time interval τ between the mw pulses, 400 ns. *Trace 2*, simulated using $g_{\|}=2.186$, $g_{\perp}=2.051$, $a_{iso}=-260$ MHz, $T_{\perp}=170$ MHz (at $g=2$) and the individual Gaussian linewidth of 55 G

$a_{iso}\approx -260$ MHz, $T_{\perp}\approx 170$ MHz (scaled to $g=2$), where a_{iso} is the isotropic hyperfine interaction (hfi) constant and $T_{\perp}$ is the perpendicular component of the anisotropic hfi tensor. The orientations of the g-tensor and the hfi tensor coincide.

The hfi parameters determined result in the effective hfi constant $|A_{\|}|\sim 200$ G, which can be directly measured from the spectrum. According to Peisach–Blumberg correlations [6], such $g_{\|}$ and $A_{\|}$ are typical for complexes with varied compositions of equatorial nitrogen and oxygen ligands, although the possibility of one equatorial methionine sulfur ligand cannot be completely excluded. In order to obtain more detailed information about the ligands to Cu^{2+} in CusF, pulsed EPR measurements were performed at the EPR positions A, B and C marked in Fig. 1. Point A corresponds to $g_{\|}$ at the Cu nuclear spin projection $m_I=-3/2$. Point B closely corresponds to $g_{\perp}$ for $m_I=-3/2$, $-1/2$ and $1/2$, and $g_{\|}$ at $m_I=3/2$ also contributes at point B. Point C is the so-called overshoot feature that corresponds to $m_I=3/2$ and a large range of $\boldsymbol{B}_o$ orientations (the angle θ between $\boldsymbol{B}_o$ and the main axis of the g-tensor is from approximately 40° to 90°).

Nitrogen ESEEM: evidence of histidine coordination

The solid line of trace 1 in Fig. 2 shows the low-frequency part of the primary ESEEM spectrum obtained at EPR position A. Three narrow lines with positive amplitude are observed in this spectrum at frequencies of 0.64, 0.88 and 1.52 MHz. One more positive line, significantly broader, has a maximum at 3.96 MHz. This

line pattern is typical for a ^{14}N nucleus when an approximate cancellation of the nuclear Zeeman and hyperfine interactions occurs at one of the electron spin projections. Indeed, in a sample of CusF enriched with ^{15}N the low-frequency pattern changes dramatically (see trace 2 in Fig. 2).

The three narrow low-frequency lines in trace 1 of Fig. 2 belong to the ^{14}N transitions within the electron spin manifold where the Zeeman/hfi cancellation takes place. The frequencies of these transitions are determined by the nuclear quadrupole interaction (nqi) only [7]:

$$\nu_o = 2k\eta;\ \nu_- = k(3-\eta);\ \nu_+ = k(3+\eta), \qquad (1)$$

where $k = e^2Qq/4h$ (e is the electron charge, Q the quadrupole moment of the nucleus, q the largest component of the electric field gradient tensor on the nucleus, and h is Planck's constant) and η is the asymmetry parameter of the electric field gradient. From the observed frequencies of 0.64, 0.88 and 1.52 MHz we can easily estimate the nqi parameters $k \approx 0.4$ MHz and $\eta \approx 0.8$ that are typical for the amino nitrogen of the imidazole ring of histidine [8].

The broad line at 3.96 MHz is often referred to as the "double quantum transition line" and corresponds to the $\Delta m = 2$ transition of ^{14}N within the other electron spin manifold [7]:

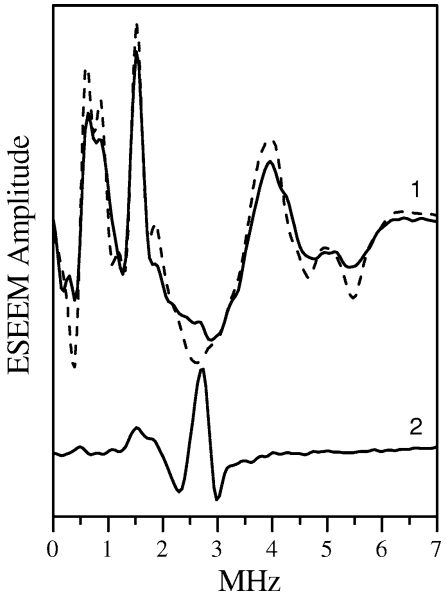

Fig. 2 *Solid lines*, primary ESEEM spectra of CusF with natural abundance of nitrogen isotopes (*trace 1*) and uniformly labeled by ^{15}N (*trace 2*). Experimental conditions for *trace 1*: mw frequency, 9.4606 GHz, mw pulses, 2×10 ns, $\boldsymbol{B}_o = 3{,}285$ G (corresponds to point B in Fig. 1). Experimental conditions for *trace 2*: mw frequency, 9.480 GHz, mw pulses, 2×10 ns, $\boldsymbol{B}_o = 3{,}286$ G (corresponds to point B in Fig. 1). The *dashed line* of *trace 1* was simulated for a single ^{14}N nucleus with $a_{iso} = 1.46$ MHz, $(T_{11}, T_{22}, T_{33}) \approx (-0.07,\ 0.37,\ -0.3)$ MHz, $(\phi_{hg}, \theta_{hg}, \psi_{hg}) \approx (0°,\ 5°,\ 0°)$, $k = 0.38$ MHz, $\eta = 0.8$ and $(\phi_{qg}, \theta_{qg}, \psi_{qg}) \approx (45°,\ 45°,\ 45°)$. The static Gaussian distribution width of a_{iso} was 0.21 MHz

$$\nu_{\Delta m=2} \approx 2\left[(\nu_N + A/2)^2 + k^2(3+\eta^2)\right]^{1/2}. \qquad (2)$$

In this expression ν_N is the Zeeman frequency of ^{14}N, and A is the effective hfi constant: $A = a_{iso} + T_{ZZ}$, where a_{iso} is the isotropic hfi constant and T_{ZZ} is the secular component of the anisotropic hfi. The two "single quantum transition" lines that belong to this manifold are usually too broad to be observed.

The ^{14}N nqi parameters determined from the ESEEM spectra indicate that at least one histidine amino acid residue is coordinated to the Cu^{2+} ion. The number of these histidine ligands can be determined with the aid of numerical ESEEM simulations. Such simulations can be performed directly for ^{14}N, but in this case a large number of parameters are involved: the hfi and nqi tensor components and the orientations of both of these tensors in the g-frame. Therefore, in order to simplify this task, we first performed numerical simulations for the ^{15}N-enriched sample.

An example of the ^{15}N ESEEM spectrum obtained at the X-band is shown in Fig. 2 (trace 2). In this spectrum, the high-frequency fundamental line of the histidine ligand(s) is located at about 2.7 MHz. It overlaps with the sum combination line (the line with negative amplitude within the frequency range from 2.8 to about 3 MHz) that has contributions from both the histidine ligand(s) and the distant protein nitrogens. Because of this overlap of the lines that belong to different nuclei, the spectra obtained at the X-band are not very suitable for simulations. Therefore, we obtained the ^{15}N ESEEM spectra in the K_u band (17.285 GHz), where the fundamental lines of the histidine amino nitrogen can be observed separately from the sum combination line.

Traces 1–3 in Fig. 3 show the K_u band ^{15}N ESEEM spectra obtained, respectively, at the EPR positions A, B and C (see Fig. 1). In these spectra, the line with a positive amplitude located at the Zeeman frequency of ^{15}N ($\nu_N \sim 2.3$ MHz in spectrum 1 and at $\nu_N \sim 2.6$ MHz in spectra 2 and 3) is the fundamental line of the distant protein nitrogens. Located symmetrically around this central matrix line is the doublet of fundamental lines of the amino ^{15}N of the coordinated histidine(s). The splittings between the lines of this doublet are about 1.8, 2.08 and 2.14 MHz in spectra 1, 2 and 3, respectively. The line with negative amplitude at $2\nu_N$ is the sum combination line contributed by both distant and ligand nitrogens. There is an additional feature at lower frequencies that partly overlaps with the low-frequency fundamental line of the ligand histidine ^{15}N. The origin of this feature is unknown.

The numerical simulations of the ^{15}N primary ESEEM spectra show that there is only one histidine amino nitrogen that contributes to the spectral lines, with a splitting of about 2 MHz. The anisotropic hfi tensor for this nitrogen is $(T_{11}, T_{22}, T_{33}) \approx (0.1,\ -0.52,\ 0.42)$ MHz, with the orientation relative to the g-frame given by the Euler angles of $(\phi_{hg}, \theta_{hg}, \psi_{hg}) \approx (0 \pm 5°,$

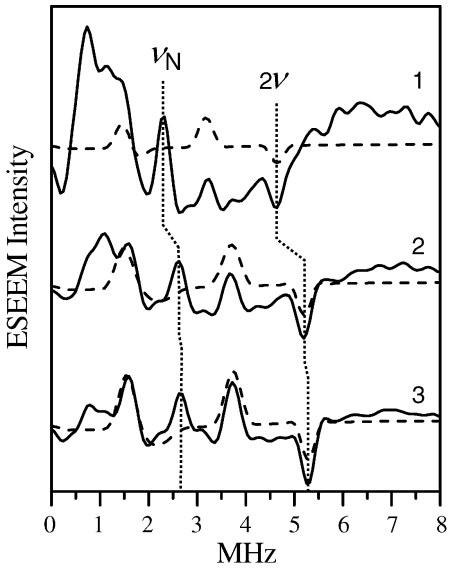

Fig. 3 *Solid traces 1*, *2* and *3*, primary ESEEM spectra of CusF uniformly labeled with ^{15}N detected at $\boldsymbol{B}_o = 5{,}370$, 6,006 and 6,100 G, respectively. These magnetic fields correspond to the electron paramagnetic resonance (*EPR*) positions A, B and C shown in Fig. 1. Experimental conditions: mw frequency, 17.285 GHz; mw pulses, 2×10 ns. *Dashed traces* are the results of numerical simulations for a single ^{15}N nucleus with $a_{iso} = -2.05$ MHz, $(T_{11}, T_{22}, T_{33}) \approx (0.1, -0.52, 0.42)$ MHz, $(\phi_{hg}, \theta_{hg}, \psi_{hg}) \approx (0°, 5°, 0°)$. The static Gaussian distribution width of a_{iso} was 0.3 MHz

$5 \pm 5°$, $0 \pm 5°$).[1] The isotropic hfi constant found in the simulations was $a_{iso} \approx -2.05$ MHz. In addition, in order to reproduce the absence of sharp features in Mims ENDOR [9] spectra (not shown) and in the sum combination line in the four-pulse ESEEM spectrum (not shown), the Gaussian distribution of $a_{iso}$with a width between the maximal slope points of 0.3 MHz was incorporated into the simulation. The spectra simulated with the described parameters are shown by dashed lines in Fig. 3. The distant nitrogen nuclei were not taken into account in these calculations, and therefore the nitrogen Zeeman line is absent in the simulated spectra. For the same reason, the simulated sum combination line amplitude is smaller than the experimental one.

The dashed line of trace 1 in Fig. 2 shows the primary ESEEM simulation for ^{14}N that used the hfi parameters given earlier for the ^{15}N-enriched sample and rescaled for ^{14}N. The nqi parameters found in the ^{14}N simulations are $k = 0.38$ MHz and $\eta = 0.8$. The orientation of the nqi tensor with respect to the g-frame is given by the Euler angles of $(\phi_{qg}, \theta_{qg}, \psi_{qg}) \approx (45 \pm 15°, 45 \pm 15°, 45 \pm 15°)$.

Finally, we should note that in addition to the experiments described previously, numerous other experiments were performed, including hyperfine sublevel correlation (HYSCORE) and ENDOR at various mw frequencies from the C to the K_u bands. All the data obtained in these studies indicate that the histidine ligand for which the previously described simulations were performed is indeed the only histidine coordinated to Cu^{2+} in this system; that is, no other histidine residues that could possibly have smaller amino nitrogen hfi are coordinated to Cu^{2+}.

ENDOR of nitrogen ligands

Unlike the amino nitrogen of the histidine ligand discussed earlier, the imino nitrogen of the same histidine is directly coordinated to Cu^{2+} and has far too strong a hfi to be detectable by ESEEM [7]. This nitrogen, as well as other possible nitrogen ligands, can be readily observed using pulsed ENDOR spectroscopy. For the ^{15}N isotope ($I = 1/2$) the expected spectra at each orientation of the complex with respect to the direction of $\boldsymbol{B}_o$ consist of two lines with the frequencies

$$\nu = |A/2 \pm \nu_N|, \tag{3}$$

where A is the orientation-dependent secular component of the hfi tensor and ν_N is the Zeeman frequency of ^{15}N.

Figure 4 shows ^{15}N Davies ENDOR [10] spectra recorded at EPR positions A, B and C. Spectrum 1, detected at $g_{\|}$, is the simplest because it corresponds to a single crystal-like situation where $\boldsymbol{B}_o$ is parallel to the $g_{\|}$ axis. There are two relatively narrow (approximately 3.5-MHz wide) lines observed in this spectrum at frequencies of about 22.3 and 27.9 MHz. The splitting of about 5.6 MHz between the lines is considerably greater than the splitting $\Delta\nu = 2\nu_N = 2.48$ MHz (for $\boldsymbol{B}_o = 2{,}875$ G) expected for the doublet of lines that belong to a single ^{15}N nucleus. Therefore, we conclude that there are two types of ^{15}N ligands coordinated to the Cu^{2+}, each contributing to one of the lines in spectrum 1. The approximately 2.5-MHz splitting within those lines is not observed because of the distribution of the nitrogen hfi in certain limits. The average effective hfi constants at $g_{\|}$ determined from spectrum 1 are thus about 45 and 56 MHz.

One of the lines in the ^{15}N ENDOR spectrum 1 belongs to the imino nitrogen in the imidazole ring of the single coordinated histidine residue that was identified in our ESEEM experiments. The intensities of the ENDOR lines in spectrum 1 are somewhat different. A nuclear transient nutation experiment, however, shows that this is caused by the difference in ENDOR enhancements. This allows us to conclude that there is only one other nitrogen coordinated to Cu^{2+}.

For a nitrogen atom σ-coordinated to one lobe of the Cu^{2+} $d_{x^2-y^2}$ orbital the hfi tensor is expected to be nearly axial, with the secular component

$$A = a_{iso} + T_{\perp}\left(1 - 3\cos^2\theta_{hB}\right), \tag{4}$$

where θ_{hB} is the angle between the main hfi axis and the direction of $\boldsymbol{B}_o$. In order to obtain the values of a_{iso} and

[1] The Euler angles as used in this work specify three consecutive rotations in the following order: (1) by ϕ around axis 3 (or z); (2) by θ around newly obtained axis 2 (or y); (3) by ψ around newly obtained axis 3 (or z).

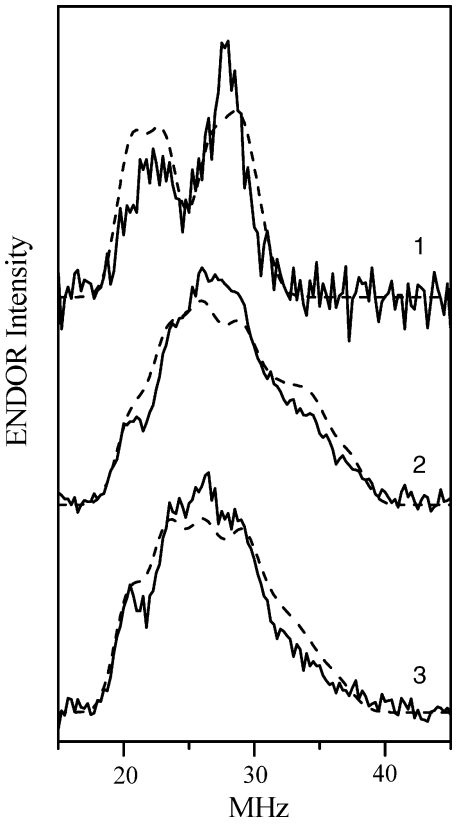

Fig. 4 Davies ENDOR spectra of CusF uniformly labeled with ^{15}N detected at $\boldsymbol{B}_o = 2{,}836$, 3,286 and 3,412 G. These magnetic fields correspond to the EPR positions A, B and C shown in Fig. 1. Experimental conditions: mw frequency, 9.480 GHz; mw pulses, 30 ns (180°), 15 ns (90°) and 30 ns (180°); time interval T between the first and second mw pulses, 20 μs; time interval τ between the second and third mw pulses, 290 ns; RF pulse duration, 5 μs. *Dashed traces* are the results of numerical simulations for two ^{15}N nuclei with the following parameters: (1) $a_{iso} = -61$ MHz, $T_\perp = 6$ MHz; (2) $a_{iso} = -47$ MHz, $T_\perp = 4$ MHz. For both nitrogens the static Gaussian distribution width of a_{iso} was 4 MHz and the main hyperfine interaction (*hfi*) axis was perpendicular to the main axis of the g-tensor

$T_\perp$ for the two nitrogen ligands, numerical simulations of the ENDOR spectra were performed. As a result of these simulations, $a_{iso} \approx -61$ MHz and $T_\perp \approx 6$ MHz were determined for one of the nitrogens, while for the other one the values $a_{iso} \approx$-47 MHz and $T_\perp \approx 4$ MHz were found. In both cases, the main axis of the hfi is in the equatorial plane of the complex and is perpendicular to the main axis of the g-tensor. The spectra simulated with these parameters are shown by dashed traces in Fig. 4.

The hfi constant $a_{iso} \approx$-61 MHz (43.6 MHz for ^{14}N) is typical for the imidazole or histidine imino nitrogen equatorially coordinated to Cu^{2+} [11–14], and therefore this hfi constant (and the high-frequency line in spectrum 1 of Fig. 4) is assigned to the histidine residue. The nature of the other nitrogen ligand that has $a_{iso} \approx$-47 MHz (33.6 MHz for ^{14}N) and gives the low-frequency ENDOR line in spectrum 1 will be discussed later in the manuscript.

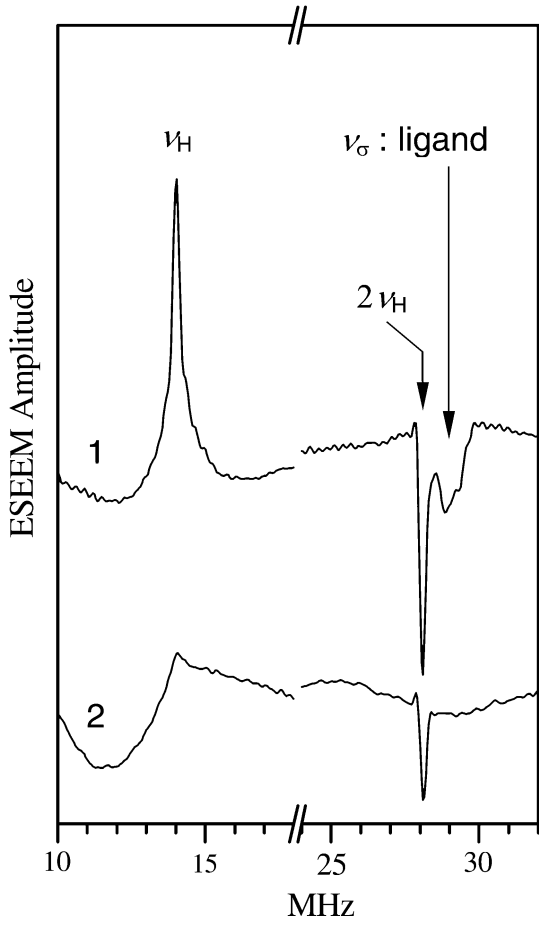

Fig. 5 High-frequency part of the primary ESEEM spectra of CusF in H_2O (*trace 1*) and D_2O (*trace 2*). Experimental conditions: mw frequency, 9.4606 GHz, mw pulses, 2×10 ns, $\boldsymbol{B}_o = 3{,}285$ G (corresponds to point B in Fig. 1)

ESEEM and ENDOR of ligand protons

In addition to the low-frequency lines caused by the interactions of the ligand nitrogens, the ESEEM spectra also contain high-frequency lines that are caused by the hfi of the distant and ligand protons (see, e.g., trace 1 in Fig. 5). The narrow fundamental line (with positive amplitude) at the proton Zeeman frequency, ν_H, and the narrow sum combination line (with negative amplitude) at $2\nu_H$ are due to the distant protons. In addition, another sum combination line is observed (denoted ν_σ in Fig. 5) that is shifted from $2\nu_H$ by about 1 MHz to higher frequencies. This shift is caused by the anisotropic hfi [7], and from the magnitude of the shift one can estimate $T_\perp \sim -6$ MHz. An anisotropic hfi constant this large indicates that the corresponding protons belong to a ligand or ligands of the copper.

Trace 2 in Fig. 5shows the primary ESEEM spectrum of a CusF sample prepared with D_2O and glycerol-d_8 instead of H_2O and protonated glycerol. One can see that in this spectrum the ligand ν_σ line has disappeared completely. In a similar experiment where D_2O and protonated glycerol were used (not shown), the ν_σ line

amplitude was about half of that in trace 1. These observations indicate that the ligand ν_σ line belongs to exchangeable protons.

In order to identify the molecular fragment containing these deuterons (OD, ND, and SD), the deuteron quadrupole coupling constant must be determined. This constant can be determined from quadrupole splittings that are often observed for the deuteron correlation lines in HYSCORE spectra [15, 16]. An example of a HYSCORE spectrum detected at EPR position A is shown in Fig. 6a.

In a HYSCORE spectrum, to second order in the hfi and first order in the nqi, the positions of the deuteron correlation lines can be described by

$$\left(\nu_D + \Delta \pm \frac{A}{2} - P,\ \nu_D + \Delta \mp \frac{A}{2} - P\right) \quad \text{and} \quad \left(\nu_D + \Delta \pm \frac{A}{2} + P,\ \nu_D + \Delta \mp \frac{A}{2} + P\right), \tag{5}$$

where ν_D is the deuteron Zeeman frequency, A and P are, respectively, the secular components of the hfi and the nqi, and $\Delta \approx \left(T_{ZX}^2 + T_{ZY}^2\right)/8\nu_D$ is the second-order correction caused by the nonsecular anisotropic hfi components T_{ZX} and T_{ZY}. For the axial nqi tensor P is given by

$$P = \frac{3}{8}\frac{e^2Qq}{h}\left(3\cos^2\theta_{qB} - 1\right), \tag{6}$$

where $\theta_{q\boldsymbol{B}}$ is the angle between the largest component $q$of the electric field gradient tensor on the deuterium nucleus and the magnetic field $\boldsymbol{B}_o$, and Q is the quadrupole moment of the deuteron.

According to Eq. 5, the correlation peaks $(\nu_D + \Delta \pm A/2,\ \nu_D + \Delta \mp A/2)$ which would hypothetically be observed without nqi split along the line parallel to the main diagonal of the spectrum. The projection of this diagonal splitting on any of the frequency axes is equal to $2P$. In the spectrum in Fig. 6a there are three ridges crossing the main diagonal at frequencies of (3.43, 3.43), (3.59, 3.59) and (3.71, 3.71) MHz. Of these, the two low-frequency ridges are located symmetrically with respect to the Zeeman frequency $\nu_D \approx 3.51$ MHz, which shows that the anisotropic hfi of the nuclei contributing to these lines is very weak ($\Delta \approx 0$). These lines are therefore mostly due to distant matrix deuterons. The splitting between these lines (approximately 0.16 MHz) corresponds to the statistically most probable orientation with $\theta_{q\boldsymbol{B}} = 90°$. Using Eq. 6 we can then readily estimate $e^2Qq/h \approx 0.21$ MHz, a value that is characteristic of hydroxyl deuterons [8, 17].

The ridge at (3.43, 3.43) MHz is actually much broader in the antidiagonal direction than the one at (3.59, 3.59) MHz. This suggests that this ridge arises not only from the distant deuterons, but also from the ligand deuterons. The other ridge that belongs to the ligand deuterons is that at (3.71, 3.71) MHz. The quadrupole splitting between these ridges is thus about 0.28 MHz. The lowest possible estimate for the quadrupole cou-

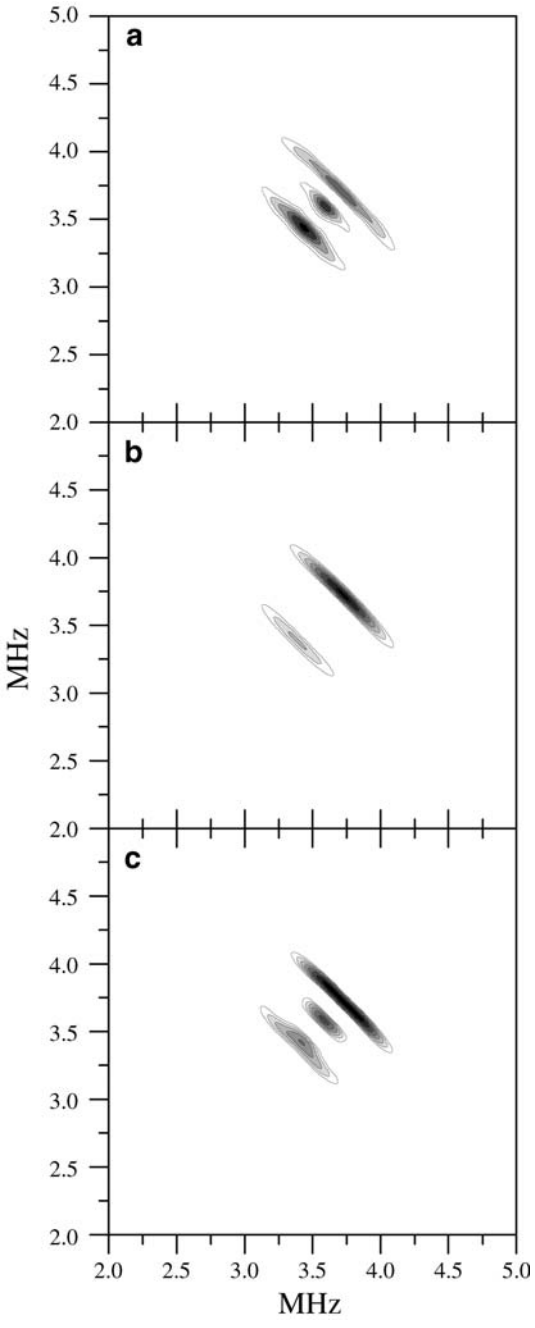

Fig. 6 **a** Hyperfine sublevel correlation (*HYSCORE*) spectrum of CusF in D_2O. Experimental conditions: mw frequency, 17.285 GHz, mw pulses, 25 ns (90°), 25 ns (90°), 21 ns (180°) and 25 ns (90°); time interval between the first and second mw pulses, $\tau = 350$ ns. **b**HYSCORE spectrum simulated for a ligand deuteron with the following parameters: $a_{iso} = -0.8$ MHz, $(T_{11},\ T_{22},\ T_{33}) \approx (-0.46,\ -1.12,\ 1.58)$MHz, $(\phi_{hg},\ \theta_{hg},\ \psi_{hg}) \approx (0°,\ 25°,\ 45°)$, $e^2Qq/h = 0.25$ MHz, and an angle between the nuclear quadrupole interaction (*nqi*) and the g-tensor axes of $\theta_{qg} = 0°$. The static Gaussian distribution width of a_{iso} was 0.4 MHz. **c**HYSCORE spectrum simulated for a ligand deuteron (as in **b**) and 12 orientationally uncorrelated remote deuterons at a distance of approximately 4 Å ($T_\perp = -0.19$ MHz), with $a_{iso} = 0$ MHz and $e^2Qq/h = 0.25$ MHz

pling constant that can be obtained from this splitting (corresponds to $\theta_{q\boldsymbol{B}}=0°$) is $e^2Qq/h\approx0.19$ MHz.

In order to obtain more accurate estimates of the hfi and nqi parameters of the ligand protons(s) or deuteron(s), numerical simulations of the primary ESEEM and HYSCORE spectra were performed. As we have already seen, the HYSCORE spectra of the sample with D_2O and glycerol-d_8 are sensitive to the quadrupole coupling constant and the orientation of the nqi tensor axis of the ligand deuteron(s). The shape of the sum combination line in the sample with H_2O is sensitive to the anisotropic hfi tensor components and the orientation of the anisotropic hfi tensor. In addition, we recorded and simulated ^{2}D Mims ENDOR [9] spectra because the orientation dependence of the ENDOR line amplitudes is different from that of the ESEEM lines. This difference allows one to improve the accuracy of the isotropic hfi estimates. Finally, the number of ligand deuterons can be found from comparison of the amplitudes of the fundamental lines due to these deuterons in experimental and simulated primary ESEEM spectra.

The simulations resulted in the following deuteron hfi and nqi parameters: $a_{iso}=-0.8\pm0.1$ MHz; the anisotropic hfi tensor components $(T_{11}, T_{22}, T_{33})=(-0.46, -1.12, 1.58)\pm(0.03, 0.03, 0.06)$ MHz; $e^2Qq/h=0.24\pm0.01$ MHz. The hfi parameters rescaled for ^{1}H are as follows: $a_{iso}=-5.2\pm0.6$ MHz; $(T_{11}, T_{22}, T_{33})=(-3, -7.3, 10.3)\pm(0.2, 0.2, 0.4)$ MHz. The orientation of the hfi tensor with respect to the g-frame is given by the Euler angles $(\phi_{hg}, \theta_{hg}, \psi_{hg})\approx(0°, 25°, 45°)\pm(5°, 2°, 5°)$. The main axis of the nqi tensor was found to be practically parallel (within 20°) to the $g_{\|}$ axis. The experimental ESEEM amplitude could only be reproduced when two deuterons (or protons) were included in the simulation.

The simulated HYSCORE spectra (without and with distant deuterons) are shown in Fig. 6b and c. Figure 7a shows examples of experimental and simulated ^{2}H primary ESEEM and Mims ENDOR spectra, while Fig. 7b shows the fitting of the proton sum combination line in the primary ESEEM spectra. The primary ESEEM simulations in Fig. 7a included the distant matrix deuterons that were modeled by 25 deuterons at a distance of 4 Å. In the HYSCORE simulation in Fig. 6c that was only sensitive to the relative number of the ligand and

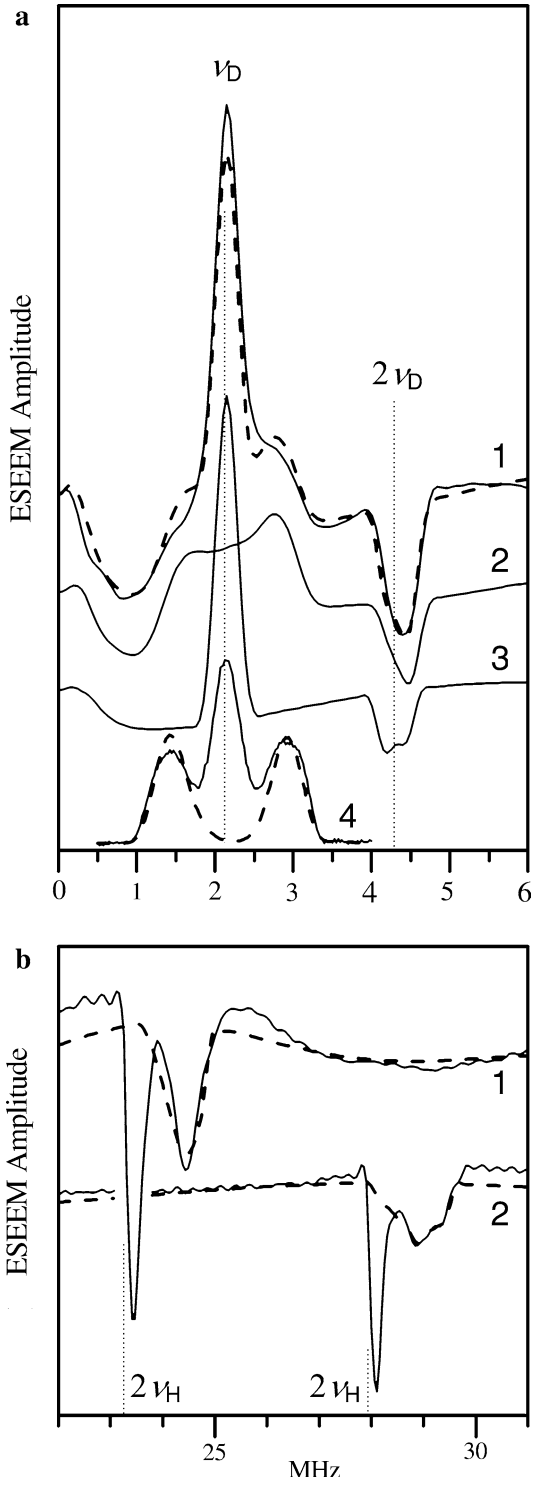

Fig. 7 **a** *Solid trace 1*, spectrum of ^{2}D primary ESEEM obtained after the division of the primary ESE decay in the CusF sample prepared with D_2O and glycerol-d_8 by the decay in the sample with H_2O and protonated glycerol. Experimental conditions: mw frequency, 9.4606 GHz, mw pulses, 2×10 ns, $\boldsymbol{B}_o=3{,}285$ G (corresponds to point B in Fig. 1). *Dashed trace 1*, simulated for two ligand deuterons with the same hfi and nqi parameters as those in Fig. 6b and 25 remote (matrix) hydroxyl deuterons at the distance of 4 Å (same as in Fig. 6c). The separate ESEEM spectra of the ligand and matrix deuterons are shown by *traces 2* and *3*, respectively. *Solid trace 4*, ^{2}D Mims ENDOR spectrum of the CusF sample prepared with D_2O and glycerol-d_8. Experimental conditions: mw frequency, 9.4606 GHz, mw pulses, 3×15 ns, $\boldsymbol{B}_o=3{,}285$ G (corresponds to point B in Fig. 1), time interval between the first and second mw pulses, $\tau=250$ ns; RF pulse duration, 55 μs. *Dashed trace 4*, simulated for ligand deuterons with the same parameters as in *traces 1* and *2*. **b** *Solid traces 1* and *2*, proton sum combination line region of the primary ESEEM spectra of CusF obtained at the EPR positions A ($\boldsymbol{B}_o=2{,}740$ G) and B ($\boldsymbol{B}_o=3{,}285$ G), respectively. Experimental conditions: mw frequency, 9.4606 GHz, mw pulses, 2×10 ns. *Dashed traces*, simulated for two ligand protons with $a_{iso}=-5.2$ MHz, $(T_{11}, T_{22},$

the distant nuclei, one ligand deuteron and 12 distant deuterons were used (i.e., the proportion was approximately the same as in Fig. 7a).

The nqi coupling constant found in our simulations is typical for a hydroxyl deuteron (e.g., in the case of an ND group it would be less than 0.2 MHz [8, 17], and in the case of an SD group $e^2Qq/h \approx 0.15$ MHz [17]). This, and the fact that two such deuterons were found, testifies in favor of a single water molecule or two hydroxyl groups being coordinated to the Cu^{2+} center. Indeed, the anisotropic hfi parameters for the ligand protons (deuterons) are similar to those found for equatorial water ligands in the Tutton salt doped with Cu^{2+} [18]. The a_{iso} value found here is about 5 times greater than that in $[Cu(H_2O)_6]^{2+}$[18], but this latter value may be sensitive to the orientation of the HOH plane with respect to the equatorial plane of the complex.

Discussion

We have characterized the equatorial ligands to the Cu^{2+} center in the CusF protein using a combination of CW EPR and pulsed EPR/ENDOR experiments. Two nitrogen ligands were found, which we will denote $N_{(1)}$ and $N_{(2)}$. One of these ligands, $N_{(1)}$, is the imino nitrogen in the imidazole ring of a histidine residue. The origin of the other ligand, $N_{(2)}$, must be discussed. Since we did not observe any neighboring NH protons, the N-terminal amino group and any lysine side chains can be excluded from consideration. Thus, a deprotonated peptide backbone nitrogen is the most likely candidate for $N_{(2)}$.

Deprotonated peptide nitrogens almost invariably have a planar coordination geometry [19] and are similar in this respect to the imidazole imino nitrogen of a histidine. In spite of this, the absolute value of the hfi constant for $N_{(2)}$ is considerably smaller than that for $N_{(1)}$: $a_{iso} \approx -47$ MHz versus $a_{iso} \approx -61$ MHz (for ^{15}N in both cases). In order to rationalize this observation, recall that the values of a_{iso} are mostly determined by the hybridization of the bonding nitrogen orbital (the lone pair orbital) and by the spin density $\rho_N$delocalized to this orbital from the central Cu^{2+} ion [14]. For a hybrid orbital being a mixture of 2*p* and 2*s*orbitals the isotropic hfi constant is

$$a_{iso} \approx \left[a_s c_s + a_p(1 - c_s)\right]\rho_N, \tag{7}$$

where $a_s \approx -2{,}160$ MHz [20], $a_p \approx -70$ MHz [20] and c_s is the *s* character of the hybrid orbital. For a nitrogen with planar coordination geometry $c_s = \cot^2(\theta_{CNC}/2)$, where θ_{CNC} is the C–N–C bond angle. For the histidine imino nitrogen $\theta_{CNC} \approx 105°$ [21], which gives $c_s \approx 0.59$ and the hybridization $sp^{0.7}$. For the deprotonated amide nitrogen with $\theta_{CNC} \approx 126°$ [22, 23], one easily calculates $c_s \approx 0.26$ and the hybridization $sp^{2.8}$. Thus, the *s* character of the lone pair orbital of $N_{(2)}$ is significantly less than that of $N_{(1)}$, which explains the difference in the hfi constants of these nitrogen ligands. Substituting these *s* characters and the experimental hfi constants in Eq. 7, we can estimate $\rho_N \approx 4.7\%$ for $N_{(1)}$ and 7.7% for $N_{(2)}$.

The anisotropic hfi constant can be approximately represented as a sum of two terms:

$$T_\perp \approx -\frac{g\beta g_n \beta_n}{R_{CuN}^3}\rho_{Cu} + b_p(1 - c_s)\rho_N, \tag{8}$$

where *g* and g_n are the electronic and nuclear g-factors, respectively, β is the Bohr magneton, $\beta_n$is the nuclear magneton, R_{CuN} is the distance between Cu^{2+} and the ^{15}N ligand nucleus, ρ_{Cu} is the spin density on Cu^{2+}, and $b_p \approx 70$ MHz [20] is the value of $T_\perp$ that would be observed if the whole spin density were localized on a 2*p* orbital of ^{15}N. For four-coordinated Cu^{2+} with nitrogen and oxygen ligands, the value of ρ_{Cu} may be roughly estimated to be about 0.7–0.8 (because about 5–7% of the spin density may be transferred to each nitrogen ligand (see earlier), and about 5% can be transferred to each oxygen ligand [24]). With $R_{CuN} \approx 1.8$–2.1 Å, the first term in Eq. 8 is about 0.9 ± 0.2 MHz. The second term is considerably greater and is between 1.4 and 4 MHz, depending on hybridization. Therefore, the total anisotropic hfi constant on the order of $T_\perp \approx 3.6 \pm 1.5$ MHz can be expected for ^{15}N ligands. This estimate is in reasonable qualitative agreement with the values found for $N_{(1)}$ and $N_{(2)}$ from the experimental ENDOR spectra.

In addition to the two nitrogen ligands already discussed, there is a single water molecule or possibly two hydroxyl groups coordinated to the Cu^{2+} center, as two exchangeable protons are observed with the appropriate characteristics for this assignment. If two hydroxyl groups are involved they would most likely be from serine, threonine or tyrosine side chains. In the case of a single water ligand, a fourth equatorial ligand would be required. This ligand, however, has not been observed, and the only information about it is of negative nature: that this ligand is not a nitrogen atom, since otherwise it would be observed by ENDOR.

Three of the histidines in CusF are found at the third, fourth and fifth positions of the processed CusF protein [2]. This series of amino acids has the potential to form a copper binding motif consisting of an N-terminal X_{aa}–X_{aa}–His sequence that has been termed the ATCUN [amino-terminal Cu(II) and Ni(II)] motif [25]. The ATCUN motif coordinates copper through an imino nitrogen of an imidazole side chain of the third amino acid in the sequence, through the deprotonated backbone amides of the second and third amino acids, and through the N-terminal amine [25]. Although the sequence of CusF may fit the consensus for this copper binding motif, it does not appear that CusF utilizes this motif for binding copper for the following reasons:

1. Only two nitrogens are involved in copper coordination in CusF, while the ATCUN motif has four coordinating nitrogens.

2. A ligand(s) which is either water or two hydroxyl groups is found in CusF, on the basis of the observation of the two exchangeable protons. The ATCUN motif does not include equatorial oxygen ligands.
3. A triple mutant of CusF to change the three histidines to arginine (H25R/H26R/H27R) has been prepared, and the EPR spectrum of this mutant looks very similar to the wild-type protein (data not shown). This observation suggests that none of these three histidines near the N-terminus of the protein provide the imidazole ligand to copper.

Thus, we conclude that copper coordination in CusF is not through a typical ATCUN motif.

Only one histidine in CusF, His58, is highly conserved among the hypothetical copper/silver transport systems in other organisms, and therefore it is a good candidate for the imidazole copper ligand. It is also possible that the histidine ligand is from the C-terminal affinity purification tag, and experiments will be done in the future to rule out this possibility. However, the optional fourth ligand mentioned earlier is potentially a carboxylate, and carboxylate-bearing side chains from either aspartate or glutamate are commonly found adjacent to His58 in CusF homologs. We speculate that a candidate for the deprotonated backbone amide would then be the amide of this aspartate or glutamate residue. The experiments done in this investigation also do not completely exclude a methionine ligand, because we have not carried out high-field ENDOR experiments with ^{33}S-labeled methionines; such investigations will be possible in the future with the now-available K_a-band pulsed EPR spectrometer.

The visible absorption spectrum of CusF shows a maximum at approximately 510 nm. Absorption at approximately 500 nm in tetragonal complexes of Cu^{2+} usually needs four nitrogen ligands [19, 26], and therefore the ligands experimentally determined in CusF so far would not be predicted to produce the observed spectra. It is possible that another ligand that we have not yet identified confers these properties, and future experiments will be directed towards obtaining a complete description of the coordination environment of the copper.

A search of the Scripps Metalloprotein Database [27] (http://www.scripps.edu/research/metallo/) of a four-coordinate copper complex that would contain only one histidine ligand and no cysteine ligands matched only one site in one protein, human ceruloplasmin [28]. This copper is one of two "labile" coppers bound by ceruloplasmin and the ligands are a histidine imidazole (residue 940), a glutamate carboxylate (residue 935) and two oxygen atoms from an aspartate carboxylate (residue 1,025). On the other hand, in a recent pulsed EPR study of Cu^{2+} surface binding sites in bacterial photosynthetic reaction centers, the Cu^{2+} ion was found to be coordinated by an imino nitrogen of a histidine residue and a peptide nitrogen [29]. Although no other (non-nitrogen) ligands, including H_2O or OH, were described in that work, at least the nitrogen coordination obtained there is similar to the one obtained in this work for CusF.

Similar nitrogen coordination was also observed in a single-crystal study of Cu^{2+} doped bis(*l*-histidinato)cadmium dihydrate [30] where one histidine molecule provided its peptide nitrogen and imidazole imino nitrogen as ligands to the Cu^{2+} ion. It is noteworthy that the hfi parameters of the histidine imidazole amino nitrogen found in that work [$a_{iso} = 1.61$ MHz and (T_{11}, T_{22}, T_{33})≈(−0.1, 0.36, −0.26) MHz] are very close to those determined here [$a_{iso} = 1.46$ MHz and (T_{11}, T_{22}, T_{33})≈(−0.07, 0.37, −0.3) MHz for ^{14}N]. The orientations of the hfi tensors relative to the g-frames are also in qualitative agreement: in both cases the axis of T_{33}makes the smallest angle with the axis of $g_{\|}$ (10° or less in this work and about 38° in Ref. [30]). The orientation of the nqi tensor relative to the g-frame in this work is also comparable to that found in Ref. [30]. These similarities may indicate that the orientations of the histidine imidazole ring relative to the Cu–N(imino) vector are similar in both cases.

The structural characterization of the Cu^{2+} complex in CusF is the first step in elucidating how periplasmic copper is handled by this protein and providing insight into its role in vivo. However, although this work reveals some of the structural details of the Cu^{2+} complex, a full understanding has not yet been attained, and thus further studies including structural characterization and studies of metal specificity and affinity are required to enhance our understanding of this system.

Acknowledgements We thank Joshua Kittleson for assistance with sample preparation. The authors acknowledge the NSF funding (DBI-9604939) for construction and modification of the pulsed EPR spectrometer used in this work.

References

1. Franke S, Grass G, Nies DH (2001) Microbiology 147:965–972
2. Franke S, Grass G, Rensing C, Nies DH (2003) J Bacteriol 185:3804–3812
3. Rensing C, Grass G (2003) FEMS Microbiol Rev 27:197–213
4. Gupta A, Phung LT, Taylor DE, Silver S (2001) Microbiology 147:3393–3402
5. Astashkin AV, Raitsimring AM, Kennedy AR, Shokhireva TK, Walker FA (2002) J Phys Chem A 106:74–82
6. Peisach J, Blumberg WE (1974) Arch Biochem Biophys 165:691–708
7. Dikanov SA, Tsvetkov YD (1992) Electron spin echo envelope modulation (ESEEM) spectroscopy. CRC Press, Boca Raton
8. Edmonds DT (1977) Phys Rep 29:234–290
9. Mims WB (1965) Proc R Soc Lond Ser-A 283:452
10. Davies ER (1974) Phys Lett A 47:1–2
11. Vancamp HL, Sands RH, Fee JA (1981) J Chem Phys 75:2098–2107
12. Polt R, Kelly BD, Dangel BD, Tadikonda UB, Ross RE, Raitsimring AM, Astashkin AV (2003) Inorg Chem 42:566–574
13. Roberts JE, Cline JF, Lum V, Freeman H, Gray HB, Peisach J, Reinhammar B, Hoffman BM (1984) J Am Chem Soc 106:5324–5330

14. Iwaizumi M, Kudo T, Kita S (1986) Inorg Chem 25:1546–1550
15. Raitsimring AM, Pacheco A, Enemark JH (1998) J Am Chem Soc 120:11263–11278
16. Raitsimring AM, Astashkin AV, Feng CJ, Enemark JH, Nelson KJ, Rajagopalan KV (2003) J Biol Inorg Chem 8:95–104
17. Semin GK, Babushkina TA, Iakobson GG (1975) Nuclear quadrupole resonance in chemistry. Wiley, New York
18. Atherton NM, Horsewill AJ (1979) Mol Phys 37:1349–1361
19. Sigel H, Martin RB (1982) Chem Rev 82:385–426
20. Zhidomirov GI, Schastnev PV, Chuvylkin ND (1978) Quantum-chemical calculations of magnetic resonance parameters. Nauka, Novosibirsk
21. Ashby CIH, Cheng CP, Duesler EN, Brown TL (1978) J Am Chem Soc 100:6063–6067
22. Freeman HC, Taylor MR (1965) Acta Crystallogr 18:939
23. Diaddario LL, Robinson WR, Margerum DW (1983) Inorg Chem 22:1021–1025
24. Getz D, Silver BL (1974) J Chem Phys 61:630–637
25. Harford C, Sarkar B (1997) Acc Chem Res 30:123–130
26. Prenesti E, Daniele PG, Prencipe M, Ostacoli G (1999) Polyhedron 18:3233–3241
27. Castagnetto JM, Hennessy SW, Roberts VA, Getzoff ED, Tainer JA, Pique ME (2002) Nucleic Acids Res 30:379–382
28. Zaitseva I, Zaitsev V, Card G, Moshkov K, Bax B, Ralph A, Lindley P (1996) J Biol Inorg Chem 1:15–23
29. Utschig LM, Astashkin AV, Raitsimring AM, Thurnauer MC, Poluektov OG (2004) J Phys Chem B 108:11150–11156
30. Colaneri MJ, Peisach J (1995) J Am Chem Soc 117:6308–6315